Mechanical response of $CH_3NH_3PbI_3$ nanowires

L. Ćirić,[1] K. Ashby,[1,a)] T. Abadie,[1] M. Spina,[1] M. Duchamp,[2] B. Náfrádi,[1] M. Kollár,[1] L. Forró,[1] and E. Horváth[1]
[1]*Laboratory of Physics of Complex Matter, Ecole Polytechnique Fédérale de Lausanne, 1015 Lausanne, Switzerland*
[2]*School of Materials Science and Engineering, Nanyang Technological University, Singapore 639798*

(Received 21 January 2018; accepted 26 February 2018; published online 12 March 2018)

We report a systematic study of the mechanical response of methylammonium lead triiodide $CH_3NH_3PbI_3$ nanowires by employing bending measurements using atomic force microscope on suspended wires over photo-lithographically patterned channels. Force-deflection curves measured at room temperature give a Young's modulus between 2 and 14 GPa. This broad range of values is attributed to the variations in the microcrystalline texture of halide perovskite nanowires. The mechanical response of a highly crystalline nanowire is linear with force and has a brittle character. The braking modulus of 48 ± 20 MPa corresponds to 100 μm of radius of curvature of the nanowires, rendering them much better structures for flexible devices than spin coated films. The measured moduli decrease rapidly if the NW is exposed to water vapor. https://doi.org/10.1063/1.5023115

The family of organic-inorganic halide perovskites, in particular, methylammonium lead triiodide $CH_3NH_3PbI_3$ (abbreviated as $MAPbI_3$), is one of the most recently studied materials for photovoltaic (PV) and optoelectronic applications. Based on $MAPbI_3$, solar cell devices with power conversion efficiencies (PCE) up to 22%[1] have been developed in a short period of time and now small-scale laboratory prototypes are reaching comparable performances as thin film CdTe solar cell or silicon based PVs.[2] Such high efficiency is due to the exceptional optoelectronic properties of the material, such as a broad absorption in the visible range, a 1.55 eV direct band gap,[3] a low exciton binding energy,[4] and a relatively large carrier mobility.[4,5] On the other hand, the PCE of perovskite based devices is still limited by the presence of defects, both inside the grains and at the grain boundaries. There is a consensus, that further studies are required for a better control of the microstructural morphology and chemical stability of the material.

In the process of making high quality crystals in order to grasp the pristine properties of $MAPbI_3$, a new form of the $MAPbI_3$ material was discovered, namely, the $MAPbI_3$ nanowire ($MAPbI_3$NW) (referred as NWs). The NWs produced by a relatively simple one step solution based deposition method, baptized as slip-coating.[6] The NWs are tens of microns in length, the width varies between 100 s of nm to few microns, and the thickness is in the sub-micron range (see Fig. 1). Unfortunately, the slip-coating method does not have a precise control of the dimensions and the spatial positioning of the nanowires on a given surface. In a follow-up work, we overcome these limitations via growing the nanowire crystallites by using the peculiar guidance effect of predefined nanofluidic channels (solvatomorph graphoepitaxy method).[7] With this approach, all the morphological parameters could be controlled and, in principle, wafer sized surfaces could be covered with NWs. Beyond the beauty of these nanostructures,[8] it has turned out that they have excellent photoconductive properties. Combined with graphene and carbon nanotubes in a non-optimized device configuration, these heterostructures have shown outstanding responsivity, as high as 10^6 A/W.[9,10] Therefore, a better control of growth at the nanoscale will allow a greater functional integration of NWs compared to their granular thin-film-type counterparts. For example, there is a strong tendency to integrate halide perovskites thin films in flexible optoelectronic devices such as solar cells, photodetectors and LEDs. For these requirements, the organic-inorganic halide nanocrystallites embedded between the various selective electrodes are more suitable, because they can withstand larger mechanical impacts, as well as the thermal dilatation induced mechanical stresses in flexible devices. The

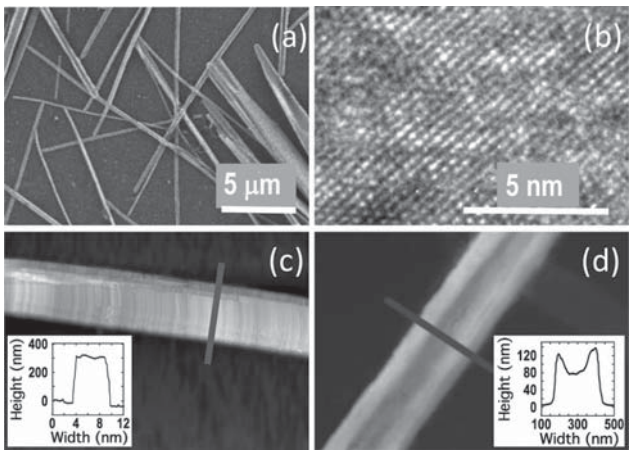

FIG. 1. (a) Typical set of $MAPbI_3$ nanowires produced by a slip coating method[6] (see the text) and imaged by SEM. (b) High resolution TEM image of a NW showing its crystallinity with some disorder. In (c) and (d) the AFM images show the width and height profiles given in the insets (at the places of the linear dark bars) of two representative sets of NWs. They define an isosceles trapezoidal and non-isosceles (U-shape) cross-sectional NWs.

[a)]K. Ashby is an exchange student from University of Nottingham.

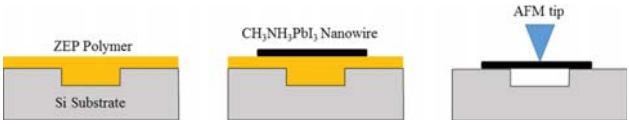

FIG. 2. Schematic representation of the workflow of preparation of suspended nanowires over trenches produced by photolithography. (Left) Once the trench is produced, the substrate is covered by ZEP and (middle) on its smooth surface $MAPbI_3$NWs are synthesized by the slip coating method. (Right) The next step consists of slowly dissolving the ZEP, where some of the NWs are bridging the trenches. From this point, the surface is scanned by AFM to locate the NWs and to determine their geometry. In three-point bending measurement with the AFM tip, the mechanical response of $MAPbI_3$NWs is determined.

nanowire form of halide perovskites can be regarded as an ideal platform for such applications. Therefore, it is of prime importance to understand the mechanical response of NWs under mechanical loads, namely, the Young's modulus (E_Y), the resilience modulus and the flexure modulus. Here, we report the measurements of these moduli for $MAPbI_3$NWs at ambient temperature in a controlled atmosphere.

The preparation of $MAPbI_3$NWs is described elsewhere.[6] A representative population of NWs is shown in Fig. 1(a). The concentration of the $MAPbI_3$ solution from which the NWs are processed influences the mean value in NWs size distribution, which could be relatively large, from tens of nanometers to few microns in width, as shown in Fig. 1(a). The crystallinity of the NWs is shown by the HRTEM image shown in Fig. 1(b). The NWs usually exhibit an isosceles trapezoidal cross-section [see Fig. 1(c)]; however, some of them appear as if two parallel NWs were joint at the middle [called as U-shaped cross section, see Fig. 1(d)]. Due to the spatial constraints during growth, the structure of these latter NWs can show a higher mosaicism.

It is well known that $MAPbI_3$ is sensitive to water vapor and this is also valid for the NW form. Exposed to air of high relative humidity ($RH > 40\%$), the material degrades and the crystallinity is lost. Most of the measurements were performed in dry nitrogen atmosphere ($RH \leq 15\%$).

The three-point bending method which is applied for measuring the mechanical response of filamentary nanostructures (nanotubes, nanowires) is called the "Swiss cheese" method, which was elaborated in our laboratory by Salvetat *et al.*,[11,12] by depositing the nanofilaments on a filtration membrane, and improved by Lee *et al.*,[13] where channels defined by e-beam lithography were used. The principle requirement of this approach is to suspend the nano-beam (wire, tube or bundle) over a micrometer sized hole or trench and perform a bending experiment with an AFM tip. By recording the force-displacement curve one is able to extract the bending modulus, breaking modulus and to estimate the domain of elastic and plastic regimes. For calculating numerical values for these moduli, one has to know the geometrical characteristics of the suspended object (length, cross section). The method has been validated on a variety of nano-filaments such as single walled carbon nanotubes (SWCNTs) and their bundles,[11] multi-walled nanotubes,[12,13] irradiated carbon nanotubes,[14] MoS_2,[15] and VO_x nanowires,[16] but also on cytoskeletal filaments (microtubules, intermediate filaments).[17,18]

The method of synthesis of $MAPbI_3$NWs asks for an unconventional preparation of the suspended NWs for the measurement of the mechanical properties by AFM. The procedure is sketched in Fig. 2. Using sequences of photolithography and dry etching steps, the arrays of 2 μm deep trenches with variable width (7, 10, 15, and 20 μm) were prepared. The range of width of the channels was adjusted to match the length distribution of the NWs. Afterwards a thin layer of ZEP520A electron beam resist was drop casted on the surface of the substrate (Fig. 2, left). Next, the NWs were synthesized on the surface of the photoresist by slip coating (Fig. 2, middle), i.e., the thin layer of the $MAPbI_3$ solution in DMF was confined to a small thickness by a glass cover slip. By choosing the slipping direction of the cover slide, the overall growth direction on the substrate of the NW can be promoted.[6] In the last step, by dissolving the resist with chloroform, the NWs softly landed on the trenches (Fig. 2, right). It has to be mentioned that we could not achieve this configuration with NWs prepared by graphoepitaxy due to technical reasons. One would have required different photoresists for the trenches and NWs growth, and different solvents, incompatible with $MAPbI_3$.

The representative examples of this processing are displayed in Fig. 3, illustrating the broad range of NWs' sizes. The length are several tens of microns, the lateral dimension varies between 0.1 to several microns, while the thickness is mostly in the nanometer range, which justifies the NW denomination for these structures. All the dimensions (suspended length, larger, and thickness) and the bending measurements were performed by using a commercial XE Park 100 AFM system with cantilevers of 0.1 N/m, 5 N/m, and 40 N/m spring constants. After a non-contact mode imaging of the NW, it was vertically deflected by the AFM tip using the contact mode option.

In this bending experiment, the NWs are considered as "clamped" to the substrate by the van der Waals force.[11] By

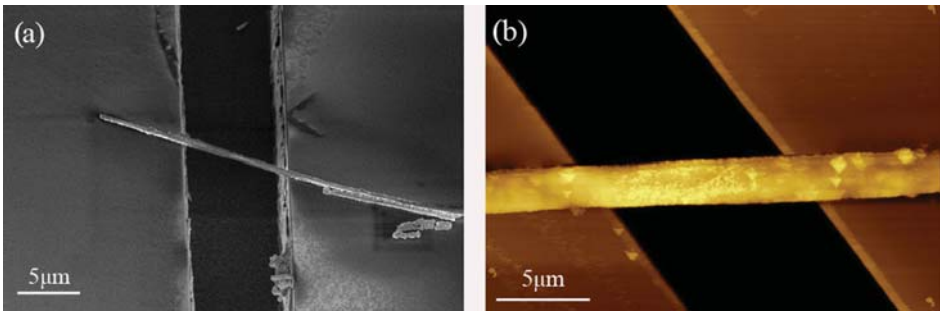

FIG. 3. Characteristic SEM (a) and AFM (b) images of $MAPbI_3$NWs suspended over trenches defined by optical lithography.

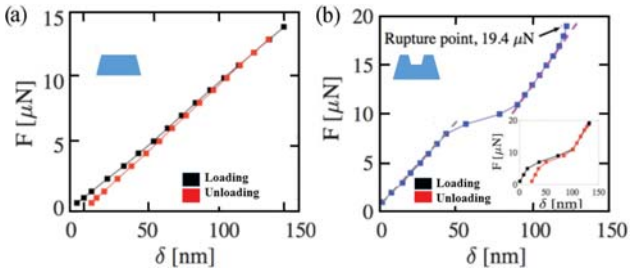

FIG. 4. Typical force-displacement (or stress-strain) curves of the $MAPbI_3$NWs. (a) Isosceles trapezoid cross-sectional NWs which show a linear response during the loading-unloading runs with a small remnant deformation. (b) Non-isosceles trapezoidal cross sectional NWs for which, after the elastic response, a plastic deformation follows which is taken over with a steeper linear regime at higher loads. At the end of the loading, this NW has broken. For another sample showing a similar response, on unloading, the plastic deformation is clearly visible in the inset. (The sketch of the profiles was determined by AFM.)

changing the set point, the bending deformation δ_B of the beam at the midpoint due to vertical load, a typical force–distance curved could be recoded on loading–unloading runs (see Fig. 4), and the numerical values for E_Y could be obtained using the following expression:

$$E_Y = \frac{FL^3}{192\delta_B I}, \tag{1}$$

where F is the force applied, L is the suspended length, δ_B is the deflection of the beam at midpoint, and I is the moment of inertia of the NW. It is important to determine with accuracy the moment of inertia which is strongly dependent on the geometry of the object. As shown above, the NWs grow rarely in regular, rectangular, or cylindrical cross sections but rather in a "belt shape," with trapezoid cross section, of a width an order of magnitude larger than the corresponding height. For every measured NW, the shape had to be measured, and I calculated. In most of the cases, I is modeled with an isosceles trapezoidal cross section expressed as $I = \frac{h^3(a^2+4ab+b^2)}{36(a+b)}$, where h is the height of the trapezoid, and a and b are the parallel sides. It is estimated that the error bar on I is in the 25%–30%.

Our experiments showed that the mechanical response of NWs can be successfully characterized by the means of AFM measurements. Nevertheless, it should be noted that the measurements were delicate due to the high sensitivity of the NWs to humidity (which was overcome by confining the AFM into a controlled atmosphere) and due to the versatile sizes and shapes of the NWs (two extreme cases are shown in Fig. 3). This required the measurement of the size of every NW independently. Typical cross sectional shapes are sketched in insert in Fig. 4. Further difficulty is the brittleness of the NWs. For lateral dimensions in the nm range, it was not possible to perform a complete force-distance run.

A typical force-displacement (or stress-strain) curve is shown in Fig. 4(a). The first important feature is that the NW exhibits relatively large domain of elastic response as a function of load. There is only a small remnant deformation (the cross section of the particular NW could be approximated by an isosceles trapezoid, as shown in the inset Fig. 4). E_Y deduced from this measurement is 14.2 ± 3.5 GPa. Due to the brittle nature of the material, the NW often brakes during the AFM force-displacement measurements. The averaged calculated fracture strength is found to be in the 50 MPa range. Our measurements also allow to extract the resilience module which is a quantity describing the maximum amount of energy a material can absorb without creating a permanent distortion. In principle, high resilience modulus of the material reduces the risk of irreversible material failure. The resilience modulus measured for the NW shown in Fig. 4(a) is of $(3.1 \pm 0.5) \times 10^4$ J m^{-3}, which could be considered as low. In comparison, aluminum has 2.3×10^5 J m^{-3}, rubber 2.11×10^6 J m^{-3} values.[19]

A second characteristic force-displacement curve is shown in Fig. 4(b). Based on the AFM images which allow to determine the cross-sectional shape of the NW, it seems that we can relate the S-shape force-displacement curve to NWs with a non-isosceles trapezoidal cross section [see the sketch in Fig. 4(b)]. The loading curve shows an elastic regime for applied force below 10 μN with a $E_{Y1} = 4.4 \pm 0.8$ GPa, then a plastic deformation follows, with a clear plateau in the force-displacement curve. For further increase of the load, a second elastic regime is found ($E_{Y2} = 6.7 \pm 1.3$ GPa). This is a typical feature of the strain hardening mechanism[20] where the movement of the crystallites under the load (in the plastic regime) takes positions which toughen the material and leads to a new elastic regime. Due to this effect, after unloading the force, a remnant plastic deformation is clearly visible [inset to Fig. 4(b)]. At the end of the loading curve, the NW in the main panel has broken. The calculated rupture or flexure modulus (using the expression 3FL/2sh2) is 48 ± 20 MPa, [where s is the average of the a and b parallel sides in the isosceles trapezoidal cross section $s = (a + b)/2$].

The feature observed in Fig. 4(b), as suggested earlier, in our view could be linked to the microcrystalline texture of the NWs observed on several NWs by TEM. Our conjecture is, that the irregular cross section of these NWs might be due to double-seeded growth (see video[7]) followed by a topotactic transformation of the translucent yellow DMF-$MAPbI_3$NW solvatomorph phase to the final $MAPbI_3$NW phase[6,7] via the evaporation of the DMF solvent. The accompanying strain induced by the significant unit cell shrinkage during the topotactic growth generates the microcrystalline structure of the wire and in consequence the S-shaped force-distance curve. In a recent theoretical paper, Yu *et al.*[21] have calculated the tensile strength of single-crystalline and polycrystalline $MAPbI_3$ samples. They obtained 15 vs 5–7 GPa for E_Y, respectively. In this frame, the large variation of E_Y for our NWs might be due to the differences of wire-to-wire crystallinity. At this point, this parameter is out of our control.

The same measuring procedure was applied for several NWs with different cross section (see Table I). The obtained values have a broad dispersion, depending probably on the crystallinity of the NWs. It has to be mentioned that exposure to high relative humidity air rapidly degraded the mechanical properties of NWs; they have E_Y well below 1 GPa (not reported in Table I) and break easily.

There are interesting reports about the special features in the mechanical response of nanowires coming from the nanometer size. For example, Chen *et al.*[22] and Wang and Li[23] have shown that the Young's modulus values depend on the diameter in the nanoscale limit. Chen *et al.*[22] have found that for ZnO nanowires E_Y strongly increases with

TABLE I. The measured values of Young modulus obtained from the linear part of the force–displacement curves for various $MAPbI_3$NWs considering an isosceles trapezoidal cross section. The estimated error bar on the absolute value of the modulus is in the 25% range due to the imprecision on the determination of the geometrical dimensions.

	Young's modulus (GPa)	Length L (μm)	Bottom width a (μm)	Top width b (μm)	Height h (μm)
1.	14.2	13.5	7.9	5.0	0.65
2.	4.4	6.4	5.8	3.8	0.48
3.	6.7	10.3	5.8	3.8	0.74
4.	2.2	7.1	6.0	2.8	0.66
5.	2.1	10.7	4.9	3.0	1.15
6.	4.4	25.7	9.3	7.2	1.40

decreasing diameter. They attributed this increase to the rearrangement of surface layers of the ZnO nanowires. DFT calculations of Wang and Li[23] did not confirm this tendency since a strong decrease of E below 60 nm was found. In another study by Duchamp[24] found a non-monotonic dependence: after an initial increase for decreasing diameter, E_Y strongly decreased below 30 nm. The present study could not contribute to this debate, since for most of the measured $MAPbI_3$NWs, only the thickness was in the submicron range.

It is informative to compare the values reported in Table I to E_Y obtained from indentation measurements on $MAPbI_3$ macroscopic crystals.[25–27] The experimentally obtained values of nano-indentation for fresh, pristine materials are in the 15–20 GPa range and E_Y rapidly decreases with the increasing humidity of the environment.[27] The highest value for NWs corroborates well with the indentation of a good bulk material. Since our measurements were performed in controlled atmosphere, we suspect that the decreased values for the NWs in respect to the highest bulk values is rather coming from the mosaicism, microcrystalline texture of the NWs than from their hydration and degradation due to water vapor absorption.

We put an emphasis on this form of $MAPbI_3$, because the charge extraction from nanowire crystalline materials is much better than from granular films, as it has been demonstrated for $MAPbI_3$NWs by the Graetzel-group.[28] The same conclusion was achieved in the case of TiO_2NWs vs. of TiO_2 nanoparticles in dye-sensitized solar cells.[29] But beyond their role in photovoltaics, the use of $MAPbI_3$NWs is getting more and more popular. From lasers, LEDs, photodetectors to thermoelectrics they find their applications.[30–36] Furthermore, the advantage of these $MAPbI_3$NWs is that they have a much lower radius of curvature (in the 10 μm range compared to mm of thin films[37]) so for devices where high mechanical flexibility is required, they could be more beneficial.

The assistance of A. Karimi is gratefully acknowledged for his help in interpreting the data. This work was supported by the ERC Advanced Grant "Picoprop" of L.F.

[1]See http://www.nrel.gov/ncpv/images/efficiency_chart.jpg for "NREL Efficiency Chart" (last accessed April 19, 2016).
[2]K. Masuko, M. Shigematsu, T. Hashiguchi, D. Fujishima, M. Kai, N. Yoshimura, and T. Yamanishi, IEEE J. Photovolt. **4**, 1433 (2014).
[3]T. Baikie, Y. Fang, J. M. Kadro, M. Schreyer, F. Wei, S. G. Mhaisalkar, and T. J. White, J. Mater. Chem. A **1**, 5628 (2013).
[4]D. B. Mitzi, J. Chem. Soc. Dalton Trans. **1**, 1 (2001).
[5]C. C. Stoumpos, C. D. Malliakas, and M. G. Kanatzidis, Inorg. Chem. **52**, 9019 (2013).
[6]E. Horváth, M. Spina, Z. Szekrényes, K. Kamarás, R. Gaal, D. Gachet, and L. Forró, Nano Lett. **14**, 6761 (2014).
[7]M. Spina, E. Bonvin, A. Sienkiewicz, B. Náfrádi, L. Forró, and E. Horváth, Sci. Rep. **6**, 19834 (2016).
[8]M. Spina, C. Grimaldi, B. Náfrádi, L. Forró, and E. Horváth, Phys. Status Solidi (a) **213**, 2017 (2016).
[9]M. Spina, M. Lehmann, B. Náfrádi, L. Bernard, E. Bonvin, R. Gaál, and E. Horváth, Small **11**, 4824 (2015).
[10]M. Spina, B. Nafradi, H. M. Tóháti, K. Kamarás, E. Bonvin, R. Gaal, and E. Horvath, Nanoscale **8**, 4888 (2016).
[11]J. P. Salvetat, G. A. D. Briggs, J. M. Bonard, R. R. Bacsa, A. J. Kulik, T. Stöckli, and L. Forró, Phys. Rev. Lett. **82**, 944 (1999).
[12]J. P. Salvetat, A. J. Kulik, J. M. Bonard, G. A. D. Briggs, T. Stöckli, K. Metenier, and L. Forro, Adv. Mater. **11**, 161 (1999).
[13]K. Lee, B. Lukić, A. Magrez, J. W. Seo, G. A. D. Briggs, A. J. Kulik, and L. Forró, Nano Lett **7**, 1598 (2007).
[14]A. Kis, G. Csanyi, J. P. Salvetat, T. N. Lee, E. Couteau, A. J. Kulik, and L. Forro, Nat. Mater. **3**, 153 (2004).
[15]A. Kis, D. Mihailovic, M. Remskar, A. Mrzel, A. Jesih, I. Piwonski, and L. Forró, Adv. Mater. **15**, 733 (2003).
[16]B. Sipos, M. Duchamp, A. Magrez, L. Forró, N. Barišić, A. Kis, and G. R. Patzke, J. Appl. Phys. **105**, 074317 (2009).
[17]A. Kis, S. Kasas, B. Babić, A. J. Kulik, W. Benoit, G. A. D. Briggs, and L. Forro, Phys. Rev. Lett. **89**, 248101 (2002).
[18]C. Guzman, S. Jeney, L. Kreplak, S. Kasas, A. J. Kulik, U. Aebi, and L. Forro, J. Mol. Biol. **360**, 623 (2006).
[19]J. R. Davis, *Tensile Testing*, edited by ASM International (ASM International, 2004).
[20]O. P. Khanna and M. Lal, *A Textbook of Material Science and Metallurgy* (Dhanpat Rai, 1987).
[21]J. Yu, M. Wang, and S. Lin, ACS Nano **10**, 11044 (2016).
[22]C. Q. Chen, Y. Shi, Y. S. Zhang, J. Zhu, and Y. J. Yan, Phys. Rev. Lett. **96**, 075505 (2006).
[23]G. Wang and X. Li, Appl. Phys. Lett. **91**, 231912 (2007).
[24]M. Duchamp, Ph.D. thesis, Ecole Polytechnique Federale de Lausanne, 2010.
[25]S. Sun, Y. Fang, G. Kieslich, T. J. White, and A. K. Cheetham, J. Mat. Chem. A **3**, 18450 (2015).
[26]Y. Rakita, S. R. Cohen, N. K. Kedem, G. Hodes, and D. Cahen, MRS Commun. **5**, 623 (2015).
[27]M. Spina, A. Karimi, W. Andreoni, C. A. Pignedoli, B. Náfrádi, L. Forró, and E. Horváth, Appl. Phys. Lett. **110**, 121903 (2017).
[28]J. H. Im, J. Luo, M. Franckevičius, N. Pellet, P. Gao, T. Moehl, and N. G. Park, Nano Lett. **15**, 2120 (2015).
[29]N. Tetreault, E. Horváth, T. Moehl, J. Brillet, R. Smajda, S. Bungener, and A. Magrez, ACS Nano **4**, 7644 (2010).
[30]H. Zhu, Y. Fu, F. Meng, X. Wu, Z. Gong, Q. Ding, and X. Y. Zhu, Nat. Mater. **14**, 636 (2015).
[31]P. Liu, X. He, J. Ren, Q. Liao, J. Yao, and H. Fu, ACS Nano **11**, 5766 (2017).
[32]K. Wang, Z. Gu, S. Liu, W. Sun, N. Zhang, S. Xiao, and Q. Song, J. Phys. Chem. Lett. **7**, 2549 (2016).
[33]S. Sun, C. Zhang, K. Wang, S. Wang, S. Xiao, and Q. Song, ACS Photonics **4**, 649 (2017).
[34]W. Deng, L. Huang, X. Xu, X. Zhang, X. Jin, S. T. Lee, and J. Jie, Nano Lett. **17**, 2482 (2017).
[35]A. B. Wong, M. Lai, S. W. Eaton, Y. Yu, E. Lin, L. Dou, and P. Yang, Nano Lett. **15**, 5519 (2015).
[36]W. Lee, H. Li, A. B. Wong, D. Zhang, M. Lai, Y. Yu, and P. Yang, PNAS **114**, 8693 (2017).
[37]K. Poorkazem, D. Liu, and T. L. Kelly, J. Mater. Chem. A **3**, 9241 (2015).